Received: 3 May 2023 | Revised: 17 August 2023 | Accepted: 23 August 2023

DOI: 10.1002/aic.18241

AIChE JOURNAL

RESEARCH ARTICLE

Soft Matter: Synthesis, Processing and Products

Janus particle amphiphilicity and capillary interactions at a fluid interface

Elton L. Correia | Sepideh Razavi

School of Sustainable Chemical, Biological, and Materials Engineering, University of Oklahoma, Norman, Oklahoma, USA

Correspondence
Sepideh Razavi, School of Sustainable Chemical, Biological, and Materials Engineering, University of Oklahoma, 100 E. Boyd Street, Norman, OK 73019, USA.
Email: srazavi@ou.edu

Funding information
Division of Chemical, Bioengineering, Environmental, and Transport Systems, Grant/Award Numbers: 1934513, CAREER-2144020

Abstract

Studying the behavior of anisotropic particles at fluid interfaces is a rapidly expanding field, as understanding how the introduced anisotropy affects the resulting properties is essential in the engineering of interfacial systems. Surface anisotropic particles, also known as Janus particles (JPs), offer new possibilities for novel applications due to their amphiphilicity and stronger binding to fluid interfaces compared to homogeneous particles. Introducing surface anisotropy creates complexity as the orientation of interfacially bound particles affects interparticle interactions, a contributing factor to the microstructure formation. In this work, we have investigated the microstructure of JP monolayers formed at the air–water interface using particles with different degrees of amphiphilicity and examined the response of the networks to applied compressions. Our findings demonstrate that JPs amphiphilicity is a crucial factor governing their orientation at the interface, which in turn dictates the complexity of the capillary interactions present and the mechanical properties of the ensuing networks.

KEYWORDS
capillary interactions, interfacial rheology, Janus particles, particle–laden interfaces

1 | INTRODUCTION

Since the initial observation of particles adsorption onto the surface of droplets and bubbles by Ramsden, which led to the stabilization of emulsions and foams, scientists have been intrigued by the behavior of colloidal particles in proximity of fluid interfaces.[1,2] The engineering of interfacial systems, composed of colloidal particles, has a wide range of applications, including but not limited to pharmaceutics, the food industry, oil recovery, and personal care products.[3–7] When particles bind to a fluid interface, the energetically unfavorable contact area between the two fluids is replaced by solid–fluid interfaces, resulting in a decrease in the overall free energy of the system. The equilibrium contact angle of a particle at a fluid interface (θ_E) can be calculated by the minimization of the free energy of the system.[8] For homogeneous particles this results in the well-known Young's equation ($\cos\theta_E = \frac{\sigma_{p1}-\sigma_{p2}}{\sigma_{12}}$) where the factors that determine the interfacial positioning of the particles (θ_E) are the interfacial tension between the two fluids (σ_{12}) and the surface tension of the particle with both fluids (σ_{p1} and σ_{p2}).[9–11] Due to their large binding energy (ΔE_d) calculated using Equation (1), relative to the thermal energy, particles are considered to be irreversibly adsorbed onto the fluid interface.[12–16]

$$\Delta E_d = \pi R^2 \sigma_{12} (1 \pm \cos\theta_E)^2 \quad (1)$$

As such, parameters including particle size (radius R), surface chemistry, and concentration have been used to alter the stability of emulsions and foams.[17–26]

Recent advances in synthesis and fabrication techniques have enabled the introduction of surface anisotropy onto colloidal particles as a means to incorporate additional functionalities into interfacial systems such as controllable assembly[27] and tunable optical properties,[28] and has enabled their use as carrying agents in drug delivery.[29] The presence of anisotropy on particle's surface results in orientation-dependent interactions between interfacially trapped

particles, which not only represents a significant advancement from a fundamental science perspective, but is also crucial from a practical standpoint, as many real-world applications involve particles with heterogeneities and nonidealities.[30–35] Therefore, the interfacial behavior in a system of particles that possess different surface chemistry on each face, also known as Janus particles (JPs), cannot be fully described by our understanding of homogeneous particles. Similar to how the equilibrium contact angle for a homogeneous particle is derived, the equilibrium position of a JP at a fluid interface can be predicted by minimizing the free energy of the system with respect to the particle's immersion angle at the interface.[36,37] Because JPs carry a dual chemistry—a polar face with a contact angle θ_P and an apolar compartment with a contact angle θ_A—they possess an amphiphilic character.[38,39] The degree of amphiphilicity, $\Delta\theta$, for a Janus particle is defined as $\Delta\theta = (\theta_A - \theta_P)/2$. The surface boundary partitioning the polar and apolar faces is indicated by the angle α; values of $\alpha = 0^\circ$ or $\alpha = 180^\circ$ correspond to a homogenous particle, whereas $\alpha = 90^\circ$ refers to a Janus particle with two equal-sized patches of different wettability.[40] For a JP ($\alpha = 90^\circ$) with a highest degree of amphiphilicity ($\Delta\theta = 90^\circ$) and with an upright orientation at the interface (Janus boundary parallel to the fluid–fluid interface, $\delta = 0$), a threefold increase in the desorption energy is predicted in comparison to a neutrally wetting homogeneous paticle.[10]

Nevertheless, JPs might not always be in an upright configuration when their orientational freedom is considered.[41] To better understand the implications of the JP orientation at fluid interfaces, one can estimate the energy required to move an interfacially bound Janus particle to the bulk using the following expression[42,43]:

$$\Delta E_d = \sigma_{12}(A_{a2}\cos\theta_A + A_{p2}\cos\theta_P - A_i) \tag{2}$$

where A_i is the fluid–fluid interfacial area removed in presence of the particle, A_{p2} and A_{a2} are the areas of the polar and apolar regions on the JP that are in contact with the apolar phase (e.g., air or oil), respectively. Furthermore, tilted particles not only are associated with changing the desorption energy of the JP, but can generate asymmetric deformations of the contact line depending on their tilt angle at the interface (δ).[43] This is due to the fact that a tilted Janus particle exposes both of its two different wetting surfaces to the subphase. The resulting asymmetric deformations of the fluid interface can thus drastically modify the dominant interparticle interactions as will be discussed further.

As in many multiphase fluidic systems, particles are incorporated to provide interfacial stability, and in some cases rendering additional functionalities, gaining a fundamental understanding of interparticle interactions taking place at the interface, and the key factors contributing to those interactions, are critical in engineering of such systems.[44] The various forms of interparticle interactions that are considered in the literature can be broadly classified into two categories: attractive and repulsive.[13] Charged colloids like silica particles,[45] when trapped at the air–water interface may experience a long-ranged repulsive interaction due to the dissociation of surface groups exposed to the polar medium, which creates an asymmetric ionic cloud around the particle relative to the interface plane.[11,46–54] In contrast, the retarded van der Waals (VDW) forces responsible for attractive interactions are typically short-ranged, effective over few tens of nanometers for micrometer-sized colloids.[55] In case of Janus particles, the cap thickness has been found to play a significant role on the strength of VDW interactions and is the dominant short-ranged force for aggregation in bulk.[56,57] However, an unexpected long-ranged attraction has been reported for interfacially trapped particles, which has been attributed to capillary forces resulting from the distortions imposed on the interface by the particles.[52,58–66] This strong long-ranged interaction has no analogy in bulk aggregation and can originate from a number of factors. Weight of the particles,[66,67] electrostatic stresses caused by the particles' dipolar field,[68,69] and particles surface roughness, chemical inhomogeneity, and shape anisotropy can cause the meniscus to take an irregular shape.[60,70–72]

A mathematical approach has been developed to model these capillary interactions, where the deformation of the contact line around the particle surface is captured as a summation of multipoles.[62] These deformations give rise to capillary interparticle interactions that can be estimated by Equation (3a) as follows[60]:

$$\frac{\Delta U_{cap}}{\pi\sigma_{12}} = H_A^2 S_A + H_B^2 S_B - H_A H_B G\cos(m_B\varphi_B - m_A\varphi_A) - \frac{1}{2}\left(m_A H_A^2 + m_B H_B^2\right) \tag{3a}$$

where $\Delta U_{cap} = U_{cap}(L) - U_{cap}(\infty)$ is the energy of capillary interaction and L is the center-to-center distance between interacting particles A and B. Considering Y as the index for particles A and B, m_Y is the mode of deformation ($m_Y = 1, 2, 3, \ldots$) corresponding to dipole, quadrupole, hexapole, etc., H_Y is the undulation amplitude for particle Y, and φ_Y is the azimuthal angle of particle Y, or the rotation angle in the interfacial plane referring to the orientation of the surface deformation. S_Y is related to the mode of deformation and approaches $m_Y/2$ at long distances, and G is the prefactor that accounts for the multipole interactions, descriptions of both are as follows:

$$S_Y = \sum_{n=1}^{\infty}\frac{n}{2}\coth[n(\tau_A + \tau_B)]A^2(n, m_Y, \tau_Y) \tag{3b}$$

$$G \equiv \sum_{n=1}^{\infty}\frac{nA(n, m_A, \tau_A)A(n, m_B, \tau_B)}{\sinh[n(\tau_A + \tau_B)]} \tag{3c}$$

$$A(n, m_Y, \tau_Y) = \sum_{k=0}^{\min(m,n)}\frac{(-1)^{m-k}(m+n-k-1)!}{(m-k)!(n-k)!k!}\beta^{m+n-2k} \tag{3d}$$

$$\beta = \exp(-\tau_Y) \tag{3e}$$

$$\tau_Y = \operatorname{arccosh}\left(\frac{L^2 + r_A^2 - r_B^2}{2Lr_Y}\right) \tag{3f}$$

where $A(n, m_Y, \tau_Y)$ is a constant independent of the approach angle, τ_Y is one of the bipolar coordinates related to the interparticle distance

and their size, and β comes from the differentiation of the integral form of $A(n,m_Y,\tau_Y)$ bringing the dependence on τ_Y to the summation. For monopole–multipole interactions, another relation must be used.[60]

For isotropic spherical particles of radius smaller than 10 μm, the monopolar contribution ($m = 0$) is much smaller than the thermal energy and can be neglected, as illustrated in Figure S1.[73] For isotropic homogeneous particles bound to a fluid interface, the dipolar contribution ($m = 1$) to the capillary interactions is also not considered since the resulting torque would rotate the particles and cancel the dipole moment generated by the distorted interface.[60] The attractive potential between two particles at a separation distance of r is therefore known to be dominated by higher order poles ($m \geq 2$), such as quadrupolar deformations, shown to scale as $U \propto r^{-4}$ at large separation distances.[60–62] This is true not only for spherical colloidal particles but also shape anisotropic particles, such as ellipsoids, for which the interparticle capillary interactions are dominated by the quadrupolar mode.[72,74–76]

Introducing the Janus character is shown to drastically change the microstructure generated by particles straddling the interface,[65] due to stronger capillary interactions.[77–79] Moreover, there is evidence that interfacially trapped JPs can interact through different polar orders (quadrupolar and hexapolar) at the same time.[80] Furthermore, the Janus character brings additional complexity when describing the resulting capillary interactions as the orientation of the JPs axis with regards to the plane of the fluid–fluid interface (δ) will affect the deformation of the contact line around the particle, and thus the terms that remain dominant in the description of the capillary interactions (i.e., $m = 1$ may not be ignored for JPs). As previously reported, JPs may assume different orientations at the air–water surface.[65,81] The distribution of tilt angles, captured for interfacially bound Janus particles, brings a unique character to JP monolayers, because in tandem with the higher order interactions such as quadrupolar ($U \propto r^{-4}$) and hexapolar ($U \propto r^{-6}$), dipolar capillary interactions ($U \propto r^{-2}$) can also be present.[43] The mixed modes of interactions may even generate strong repulsion if the interfacial undulations around interacting particles are not matching as they approach each other,[82] phenomenon previously reported for particle rafts at fluid–fluid interfaces.[83] Therefore, understanding the network of interactions with the many modes of capillary interactions present in JP monolayers is not trivial. Even more interesting is the concept that by manipulating the JPs characteristics, such as the degree of amphiphilicity, one can tune the strength of these interactions.[43,65] Thus, a JP present in a populated monolayer might experience a complex network of interactions, involving distinct modes of interaction, at different distances from its neighbors. Nevertheless, not much is known about the relation between the complex arrangement of JPs monolayers at a fluid–fluid interface and the modes of capillary interactions at play.

In this work, we focus on monolayers of Janus particles, formed at the air–water interface, to shed light on how the JP amphiphilicity affects the resulting interfacial microstructure and its mechanical response. First, we examine the mechanical differences between monolayers formed by JPs of different amphiphilicities at the air–water interface. Next, we investigate the response of such microstructures when subjected to compression/expansion stresses, as a function of their packing fraction. We then interpret the measured response in terms of how the strength and sign (i.e., attractive vs. repulsive) of the interparticle interactions present at the interface alter with the JP amphiphilicity. In order to link the role of particle amphiphilicity on the orientation of JPs at the interface, we analyze the microstructures obtained at the interface via image analysis and determine the orientation distribution of JPs at the interface. We relate the obtained information on the orientation distribution to the nature and strength of the capillary interactions involved, and the measured mechanical properties. We use Surface Evolver to estimate the desorption energy associated with such interfacially bound JPs, trapped at different orientation angles with regards to the interface, to underscore the importance of particle amphiphilicity. Next, we use the information obtained from the image analysis, on the orientation angle of the particles at the interface and the interacting neighbors, to calculate pairwise capillary interactions within the network and the energy landscape of the networks obtained with each JP amphiphilicity. Finally, we discuss the relevance of our findings to the complex capillary interactions present in JPs monolayers and the significance of the JP amphiphilicity on the capillary interactions present at the interface and its consequences for the mechanical properties of the network in response to applied stresses.

2 | MATERIALS AND METHODS

2.1 | Janus particle fabrication, surface modification, and characterization

To fabricate the Janus particles, hydrophilic silica particles (1 μm, Fiber Optic Center) were assembled onto a 2D PVC film by transferring the particles from air–water interface to the air–solid interface using a Langmuir trough.[84] Next, the monolayers were transferred to physical vapor deposition machine (Lesker Nano36 Evaporator, Kurt J Lesker) onto which a thin adhesive layer (5 nm) of titanium was deposited followed by a 10 nm layer of gold. Resulting JPs were labeled as C_0 as no further modification was carried out on the gold cap. To enhance the JP amphiphilicity, gold faces were further modified with butanethiol and octanethiol (Sigma–Aldrich) by soaking the coated films in 10 mM solution of the thiol in ethanol (Fisher Scientific) overnight. The resulting JPs were labeled as C_4 and C_8, respectively. All particles were removed from the substrate and suspended in ultrapure Deionized (DI) water via sonication, followed by a filtration using a hydrophilic PC membrane filter (10 μm, Isopore™) to remove large aggregates and gold flakes. After these steps, the dispersions were centrifuged at 3000 rpm for 5 min (Legend X1R, Thermo Scientific) followed by the aspiration of the supernatant. The JPs were set to dry under vacuum overnight. DI water (18.2 MΩ cm) used throughout the study was generated via Milli-Q® IQ 7000 Ultrapure Lab Water System (Millipore Sigma).

The JP degree of amphiphilicity ($\Delta\theta$) is quantified via the measurement of wettability on each face of the particle. Specifically, the wettability of the silica and gold faces were estimated by measuring the 3-phase contact angle of water droplets deposited on base-cleaned glass substrates and glass substrates passed through the same gold deposition and surface modification as the particles. The water-drop shape profile obtained in each measurement was fitted and analyzed using a tensiometer (Biolin Scientific), from which the 3-phase contact angle of the polar (θ_P) and apolar (θ_A) faces of the JPs were estimated.

2.2 | Monolayer preparation at the air–water interface

To prepare the particle dispersions, JPs were suspended in a 30/70 wt% water/isopropyl alcohol (Fisher Scientific) mixture at a concentration of 37.5 mg/mL. A NIMA Langmuir trough (Biolin Scientific) was filled with 160 mL of DI water and the trough area was set at 150 cm^2, that is, the open barrier state, in all experiments. To ensure the absence of impurities at the air–water interface, the trough was closed to 60 cm^2 and the change in the surface pressure (Π), defined as the difference between the air–water surface tension (σ_0) and the effective surface tension in presence of particles (σ_{eff}) was monitored. If the surface pressure remained negligible ($\Pi < 0.3$ mN/m), the experiment proceeded. The spreading solution was deposited at the interface in a dropwise fashion using a 50 µL syringe (Hamilton) where the particles spread at the interface via the action of Marangoni flows. To attain a similar range of surface pressures for all particle amphiphilicities studied, the volume of the spreading solution was adjusted to 200, 250, and 300 µL for C_0, C_4 and C_8, respectively. A 30 min wait period was considered to allow for the solvent evaporation before proceeding with the measurements. The trough area (A) was compressed at 10 mm/min and the surface pressure $\Pi(A)$ was monitored via a Wilhelmy plate. The compression was followed by an expansion of the interfacial area at the same rate to probe the hysteresis of the JP interfacial network. The monolayers were subjected to 3 cycles of compression and expansion. In conjunction with the compression–expansion cycles, an inverted microscope (IX73 Olympus) was utilized to simultaneously capture the microstructure formed by the particles at the air–water interface, using a 20× objective (6.6–7.8 WD, 0.45 NA), and through a custom-designed window machined in the center of the trough.

2.3 | Analysis of surface pressure isotherm

To extract information on the mechanical properties of the network, the resulting surface pressure isotherms were further analyzed to calculate the isothermal surface compressibility coefficient, $\kappa_0^s = -\left(\frac{\partial \Pi}{\partial \ln A}\right)_T$ of the interfacial network as a function of the JP amphiphilicity.[85] To further examine the link between JP amphiphilicity, the overall interparticle interactions experienced by the particles within the network, and the resulting surface pressures, a surface equation of state was used to interpret the surface pressure isotherms.[86] As shown by Fainerman et al., the surface pressure of a micron-sized particle monolayer can be related to the particle surface coverage and interparticle interaction parameter via the following equation:

$$-\frac{\Pi\omega_0}{kT} = \ln(1-\theta) + \theta\left(1-\frac{\omega_0}{\omega}\right) + a\theta^2 \quad (4)$$

where ω_0 is the molecular area of the solvent, ω is the fluid–fluid interfacial area occupied per particle, and θ is the particle surface coverage. Therefore, using the information on the total area occupied by the particles at any time, one can calculate θ. We estimated the total area occupied by particles assuming an arbitrary value for the surface coverage at the inflection point (θ_{IP}) of the isotherm. The Frumkin interaction parameter (a) captures the nonideality (i.e., positive for attractive and negative for repulsive interactions), and is related to the enthalpic contribution to the interactions.[86] We assumed that the $\frac{\omega_0}{\omega}$ ratio goes to 0 since $\omega \gg \omega_0$, and used both a and θ_{IP} as fitting parameters, to estimate the limiting surface coverage and interaction parameter that best represents the surface pressure data obtained for JPs with different degree of amphiphilicity. From the maximum surface coverage in 2D (i.e., θ_{IP}) that best fits the experimental data, the area occupied by the particles at the inflection point of the isotherm can be estimated. From the total area occupied by particles, we can calculate the number of particles trapped at the surface. Next, the binding efficacy of JPs can be estimated by dividing the total number of particles trapped at the interface by the total number of particles deposited at the interface from the spreading solution.

2.4 | Analysis of particle orientation distribution

To evaluate the orientation distribution of the JPs residing the air–water interface, deposition of interfacially trapped particles on a silicon wafer was carried out following an earlier work.[9] Briefly, a silicon wafer was placed at the bottom of the trough at the beginning of the experiment. After the particles were spread at the interface, a 30 min wait period was allowed for the evaporation of the spreading solvent. Next, the monolayer was compressed until a surface pressure of 5 mN/m was reached. The JP network was then transferred from the air–water interface to the silicon wafer substrate by gently aspirating the water from the side of the trough outside the barriers and lowering the interfacial plane until the particle monolayer came in contact with the silicon wafer. The deposited particles were then imaged via the environmental Scanning Electron Microscope (Thermo Quattro S field-emission SEM) equipped with a backscatter detector, which exhibits different brightness for materials of different density.

The distribution of particle orientations was obtained by analyzing ~50,000 particles, for each amphiphilicity studied, using the HEXI software via brightness thresholding of the particles.[87] Particles that showed up brighter in the SEM images (i.e., in contact with the air phase) were counted as Janus cap up and those dimmer were counted

as Janus cap down (i.e., facing toward the water subphase). To differentiate the tilted particles, we used the standard deviation of the pixel brightness in each particle as the criterion, since a wider spread in the brightness population is expected for a tilted particle compared to vertically aligned particles. More details on the particle thresholding can be found in Figure S2. Once the orientation (δ) of all particles is determined, one can calculate a 2D-alignment factor $S = \left\langle \frac{3\cos^2\delta - 1}{2} \right\rangle$ as a means of quantifying the overall orientation of the JP cap in the particle monolayers formed by different amphiphilicities.[88] To calculate a 2D alignment factor (S), the value of particle tilt angle (δ) was simply assumed to be 0°, 90°, and 180° for cap up, tilted, and cap down Janus particles, respectively. Therefore, a monolayer populated only by vertically aligned particles (cap up and cap down) corresponds to $S = 1$, whereas for a monolayer comprised of particles in sideways configuration the 2D alignment factor is $S = -0.5$.

2.5 | Calculation of desorption energy at different orientation angles via Surface Evolver

JPs possess chemical anisotropy, which generates deformations on the air–water interface due to the entrapment of particles in a tilted orientation. Vertically aligned particles will likely generate deformations associated with the surface roughness present at the Janus boundary (commonly described via quadrupolar and hexapolar modes), whereas tilted particles introduce dipolar deformations. Following the work of Rezvantalab et al.,[43] the Surface Evolver software[89] was employed to model a system of a single Janus particle straddling a fluid interface at an arbitrary orientation angle δ. The software can be used to model interfacial deformations that are induced by various forces and constraints present in the system. In our system, the surface energies, which are dependent on the wettability of the particle hemispheres, were considered the governing force. Once the geometry is created, one can refine the mesh and minimize the surface energy until convergence is achieved. The software considers the surface tension between the fluids as 1, which was converted afterwards to the surface tension of water ($\sigma_0 = 72.8\,\mathrm{mN/m}$). To model the JPs of various amphiphilicities, we set the contact angles of the hemispheres to the experimentally measured values, held the particle position constant, and incrementally increased the tilt angle. Once the mesh is converged, the contact area between each hemisphere and the subphase was exported and Equation (2) was applied to calculate the desorption energy (ΔE_d) associated with each orientation angle (δ).

3 | RESULTS AND DISCUSSION

3.1 | Janus particles degree of amphiphilicity

The degree of amphiphilicity ($\Delta\theta$) is a measure of the Janus character of the particle. In the system under study, the hydrophobicity of the gold cap was tuned by attaching thiol molecules to the surface. Therefore, by introducing thiols with longer carbon chains onto the gold cap, JP amphiphilicity can be gradually increased, while retaining the wettability on the hydrophilic silica side. Examples of water droplets formed on the unmodified glass substrate, gold coated substrate and thiol modified gold substrates, and the resulting contact angles measured in each case are provided in Figure 1. Based on this information, the degree of amphiphilicity were estimated for C_0, C_4 and C_8 particles, as provided in Table 1.

3.2 | Surface pressure isotherms

The surface pressure (Π)—area (A) isotherm for the three systems under study are provided in Figure 2A. It can be noted that each curve goes through an inflection point which is associated with an area (A_{IP}) that is smaller for C_0, intermediary for C_4, and larger for C_8. This can be attributed to each amphiphilicity having a different binding efficacy (Table 1). The binding efficacy is estimated based on the number of particles trapped at the interface divided by the number of particles deposited onto the fluid interface. Particles with higher amphiphilicities presented a higher binding efficacy, which is in agreement with previous studies on interfacial monolayers of Janus particles.[9] The area at the inflection point (A_{IP}) was then used to normalize the

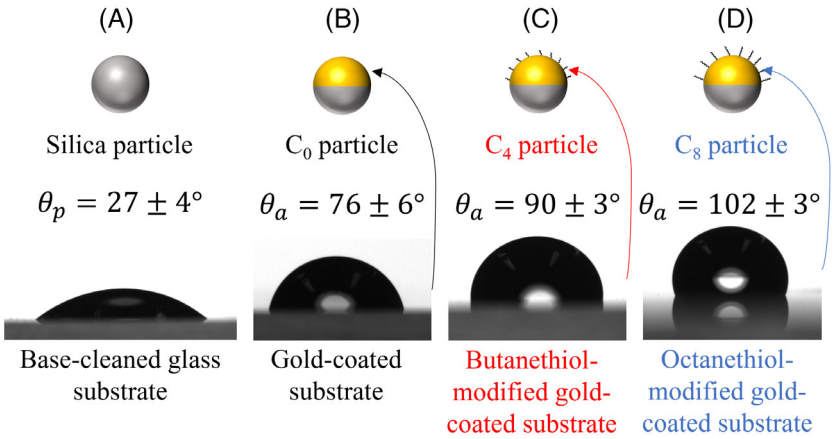

FIGURE 1 Wettability of glass substrates, modified in an analogous fashion to the particles, and measured via the contact angle of water droplets deposited on the substrate. The representative particle surfaces are also provided above each panel. From left to right, (A) the untreated base-cleaned substrate, (B) unmodified gold coated substrate, (C) gold-coated substrate modified with butanethiol, and (D) gold-coated substrate modified with octanethiol. Janus particles are composed of a hydrophilic silica surface mimicked by the glass substrate shown on panel (A) and a gold cap, unmodified or thiol-modified, as shown in panels (B)–(D).

TABLE 1 Janus particles under study and their characterization as follows: degree of amphiphilicity ($\Delta\theta$), binding efficacy at the interface, isothermal 2D compressibility modulus of the particle network, network compaction between cycles 1 and 3, and parameters obtained from the fitting of the surface pressure isotherms to the Frumkin equation of state, that is, the surface coverage at the inflection point (θ_{IP}) and the overall interparticle interaction parameter (a).

Particle	$\Delta\theta$	Binding efficacy	Maximum κ_0^s (mN/m)	% compaction from cycle 1 to 3	θ_{IP}	a
C_0	25 ± 5°	79.2%	170 ± 9	10.4%	80.0%	−0.04
C_4	32 ± 4°	85.5%	228 ± 43	9.9%	88.4%	0.59
C_8	38 ± 4°	88.3%	308 ± 47	4.7%	91.0%	1.09

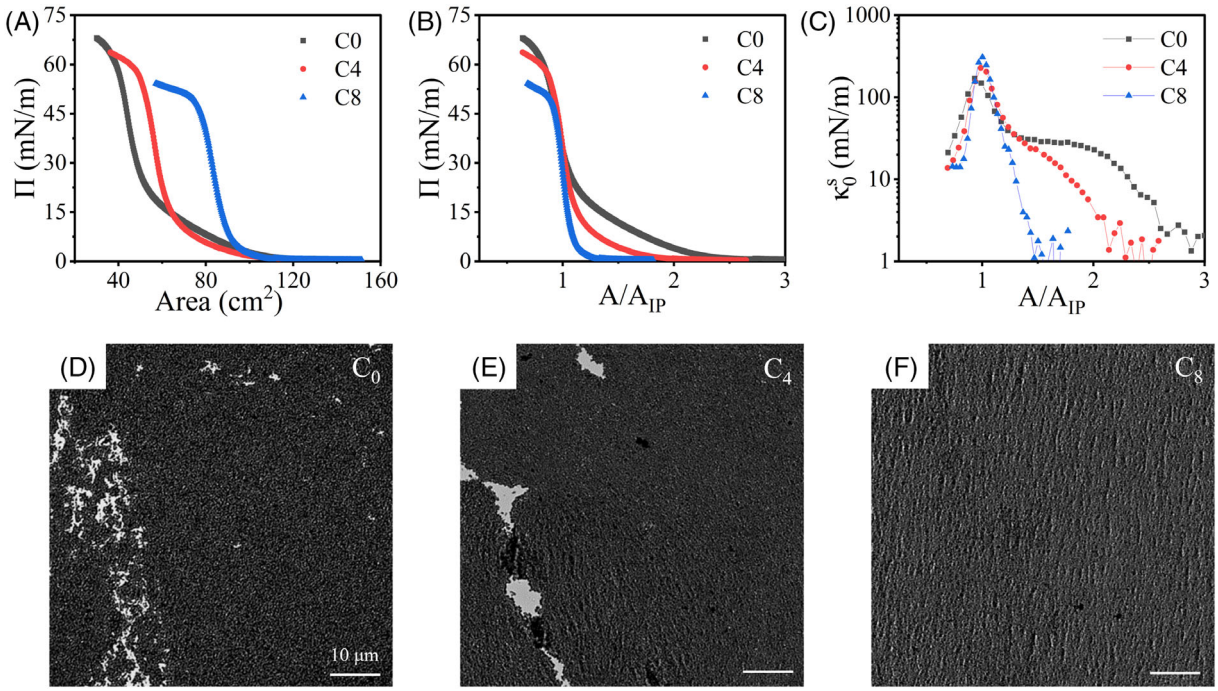

FIGURE 2 (A, B) Display the surface pressure (Π) isotherm for Janus particle monolayers of different amphiphilicity as a function of trough area (A) and area normalized by the inflection point area (A_{IP}), respectively. (C) Surface compressibility modulus (κ_0^s) of the monolayers for JPs of different amphiphilicity. Data belonging to C_0, C_4, and C_8 particles are illustrated using black squares, red circles, and blue triangles, respectively. Snapshot of monolayer beyond collapse for (D) C_0, (E) C_4, and (F) C_8. Scale bar is 10 μm.

surface area in each isotherm, results of which are displayed in Figure 2B. The inflection point of the isotherm has been associated with the point at which the monolayer has reached its maximum packing in two-dimensions. Compressing the monolayer past the inflection point of the isotherm is shown to result in the collapse of the interfacial network either by expelling the particles from the interface or buckling of the particulate layer.[90]

Comparing the three isotherms, it can be observed that by compressing the interfacial monolayers, the surface pressure picks up for C_0 Janus particles at larger normalized areas, which indicates the formation of an open fractal network due to the directional dependece of interparticle interacitons.[91] There is a clear progression from C_0 to C_4, and then to C_8, where C_8 does not resist compression up to areas close to the inflection point, which indicates a dominance of short-ranged interactions. Plotting the isothermal 2D compressibility modulus (κ_0^s) with the normalized area in Figure 2C, further illustrates that resistance to the applied compression initiates at larger normalized areas for the particle monolayer formed by the C_0 JPs, followed by the networks of C_4 and C_8 particles, respectively. It should be noted that κ_0^s reaches a maximum at the inflection point of the isotherm as expected, from which one can obtain the maximum resistance to compression exhibited by the monolayers. Surface compressibility values show a direct relationship with the degree of amphiphilicity, as shown in Table 1. This indicates that JP of higher amphiphilicity yield monolayers that exhibit a larger resistance to the applied compression when compared at the maximum particle surface coverage obtained in 2D.

After reaching their maximum resistance to compression at the inflection point, the monolayers yield to the applied stress and undergo a collapse process, which is evidenced by the "shoulder" recorded on the surface pressure isotherm. To illustrate the microstructural changes within the network in response to the applied

compressions, the corresponding videos (sped up 3×) are provided in Supporting Information. Figure 2D–F displays snapshots of the microstructure after the inflection points of the isotherms have been reached. The monolayer formed by C_0 JPs possess particle clusters that, upon compression, do not combine to form larger aggregates resulting in areas devoid of particles that persist (Figure 2D). In contrast, C_8 monolayer is more uniform and shows wrinkles once compressed beyond the collapse point (Figure 2F). It should be noted that monolayer formed by C_4 exhibits an intermediary behavior, with both characteristics, where local wrinkles are observed before the holes between clusters get filled up by particles and disappear completely (Figure 2E).

To gain an understanding on how the strength of interparticle interactions is altered by the JP amphiphilicity, we applied an equation of state, proposed by Fainerman et al.,[86] to the measured surface pressure isotherms using both the surface coverage at the inflection point (θ_{IP}) and the interaction parameter (a) as fitting parameters. The results are provided in Table 1 and are shown in Figure 3, where the comparison between the experimental data and the resulting fit are plotted for all amphiphilicities as a function of the particle surface coverage (θ), which was estimated based on the area occupied by particles at the inflection point, calculated from θ_{IP}. In agreement with the results shown in Figure 2, the surface pressure obtained for the C_0 monolayer is always higher than the other two JP amphiphilicities when compared at a similar surface coverage. In other words, obtaining similar surface pressures requires the lowest surface coverage in the case of C_0 particles. This may be due to the slightly repulsive interaction parameter ($a = -0.04$) in case of C_0 particles, which indicates that the network is overall resisting the applied compression. In contrast, C_8 particles show the lowest surface pressure at the same surface coverage, resulting from the overall attractive interactions ($a = 1.09$). Moreover, the limiting packing fraction (θ_{IP}) associated with C_0 is the lowest value ($\theta_{IP} = 80\%$), indicating a more open network,

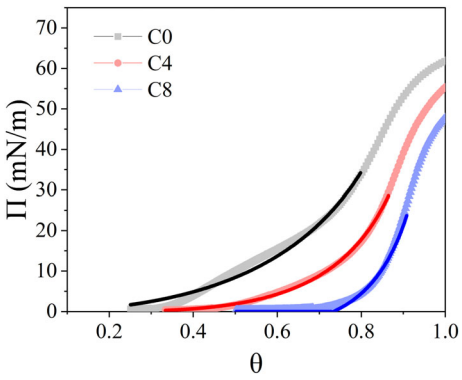

FIGURE 3 Surface pressure (Π) isotherms as a function of surface coverage of particle (θ) obtained for JP monolayers of different amphiphilicities at the air–water interface. C_0 particles are shown in black squares, C_4 particles in red circles, and C_8 particles in blue triangles. The experimental data are shown in lighter tones and the best fit from the Frumkin equation of state (Equation 4) are shown in a darker tone. The function only fits the data for $\theta \leq \theta_{IP}$ since at higher surface coverages the monolayer is not a 2D structure.

devoid of particles, which corroborates with the idea that particle rafts are not attracted to each other. On the other hand, the maximum packing obtained in monolayers formed by C_8 particles corresponds to a hexagonal closed pack arrangement in 2D and is equivalent to 91%. This difference in θ_{IP} is evidenced on the recorded videos of the monolayer compression provided in Supporting Information.

It is worth noting that the fitting on C_0 is not optimal. This could be attributed to the complexity of interactions that are occurring at different length scales, that is, interactions of different magnitude, strength, and sign may be taking place at different interparticle distances as will be discussed later.

3.3 | Isotherm hysteresis

Since interfaces are often subjected to repeated external stresses, additional analysis arises from the cycles of compression and expansion undergone by these monolayers, as they can offer valuable information regarding the hysteresis involved in these systems. Figure 4 shows the comparison between the isotherms obtained on cycle 1 and cycle 3 for interfacial layers formed by the JPs of different amphiphilicity. The data is illustrated as a function of the compression ratio (A_0/A), defined as the ratio between the initial area at the open-barrier state (A_0) and the area at any point (A) during the experiment, which can be useful with regards to hysteresis analysis.[92] From these curves we can learn information regarding the induced monolayer compaction (comparing different compressions), and overall interparticle interactions (from the differences between compression and expansion isotherms). As shown in Figure 4A, for interfacial layers formed by C_0 JPs, there is a minor shift in the isotherm toward smaller normalized trough areas from cycle 1 to 3, which could be attributed to either particle loss from the interface or the compaction of the monolayer upon compression. The former scenario is excluded in this case as the maximum pressure reached at the closed-barrier state remains the same across all three cycles.[90] For C_4 and C_8 monolayers, there is a similar shift to the right comparing the compressions in cycle 1 to cycle 3, as illustrated in Figure 4B,C. Using the inflection point from compressions 1 and 3, one can calculate the network compaction in response to cyclic deformations as $\left(A_{IP}^{3rd} - A_{IP}^{1st}\right)/A_{IP}^{1st}$, results of which are provided in Table 1.

When comparing the compression to the expansion for each cycle, C_0 monolayers behave similarly, depicted by similar shapes, regardless of the cycle number, with the expansion curve always exhibiting smaller surface pressures than the compression. Interestingly, the expansion surface pressure does not drop to 0 mN/m immediately after the area has reached values larger than the collapse area, indicating that the network is opening and exhibiting a solid-like behavior.[63] In contrast, C_4 and C_8 monolayers exhibit hysteresis at the first cycle. However, for the third cycle the compression and expansion legs of the isotherms overlap each other indicating that larger aggregates are being formed and are not breaking apart after the expansion, which could be resulting from the lack of repulsion between the particles. C_4 monolayers also experience a

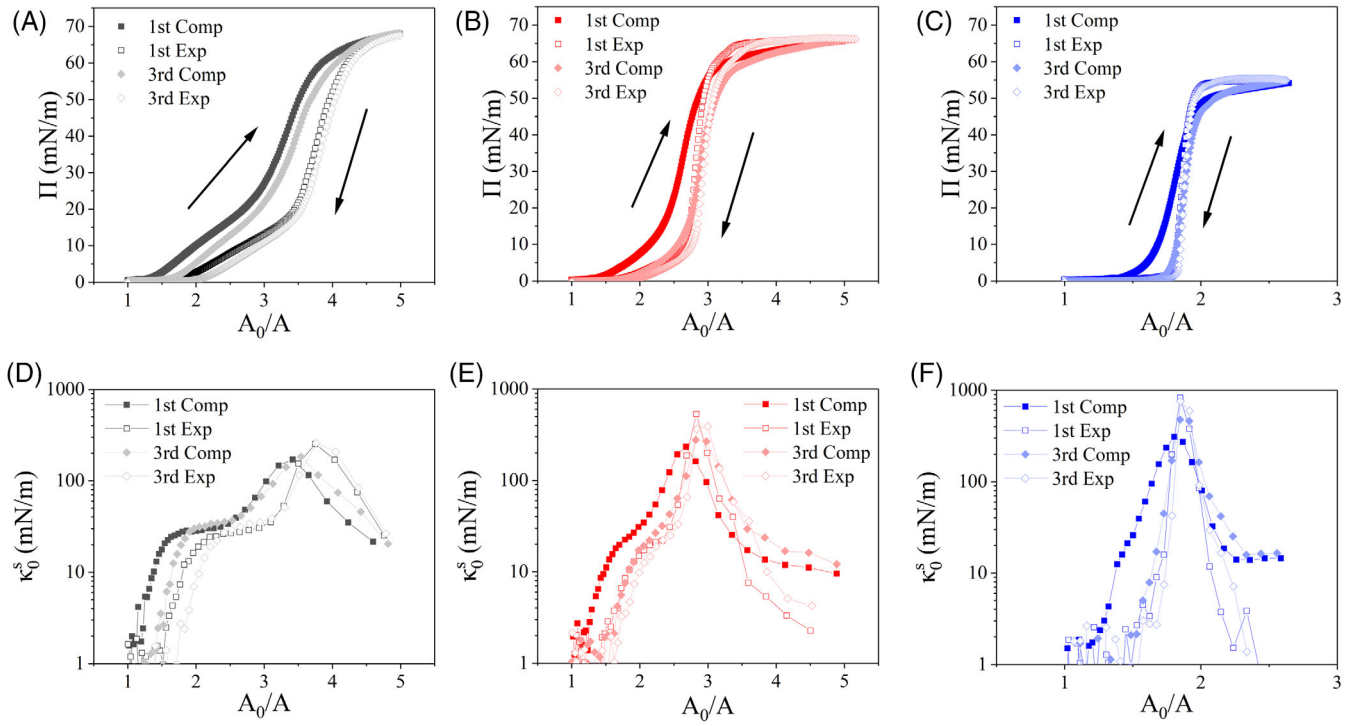

FIGURE 4 Surface pressure (Π) isotherm plotted as a function of the compression ratio (A_0/A) for compression (square closed symbols) and expansion (diamond open symbols) legs of cycles 1 and 3 for the monolayers formed by (A) C_0, (B) C_4, and (C) C_8 Janus particles; the compressional surface modulus (κ_0^s) for each particle monolayer are presented below the isotherms corresponding to (D) C_0, (E) C_4, and (F) C_8 Janus particles. Data belonging to C_0, C_4, and C_8 particles are shown in black, red, and blue color, respectively.

similar but less drastic version of the phenomenon taking place in C_0 in which the surface pressure does not instantaneously drop to 0, whereas the surface pressure for C_8 reaches 0 mN/m as soon as the area is larger than the collapse area.

When analyzing κ_0^s, for the monolayer formed by C_0, shown in Figure 4D, there are clearly two regions, corresponding to a plateau on the lower surface concentrations (on the left) and the peak at the inflection point. The fact that κ_0^s for both compression and expansion cycles have a comparable shape and similar values indicates that the particles within this monolayer are interacting repulsively, and once the expansion is taking place the same particle clusters that were resisting the compression push each other away. In contrast, for the monolayer formed by the C_8 particles, the compressibility modulus from the first compression shifts to smaller areas and remains relatively the same from the first expansion onwards as depicted in Figure 4F. This can be attributed to a large degree of compaction taking place within the monolayer, where the particles that were pushed together remain in the form of compact aggregates, due to the attractive nature of their interactions. This is also evidenced in the maximum compressional modulus where the 3rd cycle reaches a higher value (~476 mN/m) than the 1st (~308 mN/m), as the monolayer is compacted upon compression, and thus is harder to compress. Finally, the monolayer formed by C_4 particles exhibits an intermediary behavior; analogous to the C_8 system, the interfacial layer compacts to some degree in response to the applied compression in the first cycle, as shown in Figure 4B, whereas the shape of the compressional modulus is sustained indicating some repulsiveness in the interparticle interactions, as can be seen in Figure 4E.

3.4 | Microstructure analysis

To better understand the impact of JP amphiphilicity on the microstructure of the monolayers formed at the interface, imaging of the interface was conducted in tandem with the compression of the layer. The acquired data allows us to simultaneously track the surface pressure and visually inspect the resulting microstructure. When comparing the monolayers formed by JPs with different degrees of amphiphilicity, at the same surface pressure of 5 mN/m, different microstructures are shown to be present at the interface as depicted in Figure 5. The least amphiphilic C_0 JP system appears to consist of mostly open air–water areas devoid of particles, with some smaller dendritic particle chains and some larger aggregates of more densely packed particles (Figure 5A). As the particle degree of amphiphilicity is increased, by moving from C_0 JPs to C_4 JPs (Figure 5B), a decrease in the number of particle chains is observed, whereas the aggregate size and the connectivity of particle rafts increased. The packing in C_4 particles appears to be more compact in comparison with C_0 particles. For the largest amphiphilicity studied, the surface network of C_8 particles is predominantly covered by large, interconnected aggregates and the bare air–water surface area was the least in this case (Figure 5C). These results agree qualitatively with Figure 3, where the surface coverage is inversely proportional to the degree of

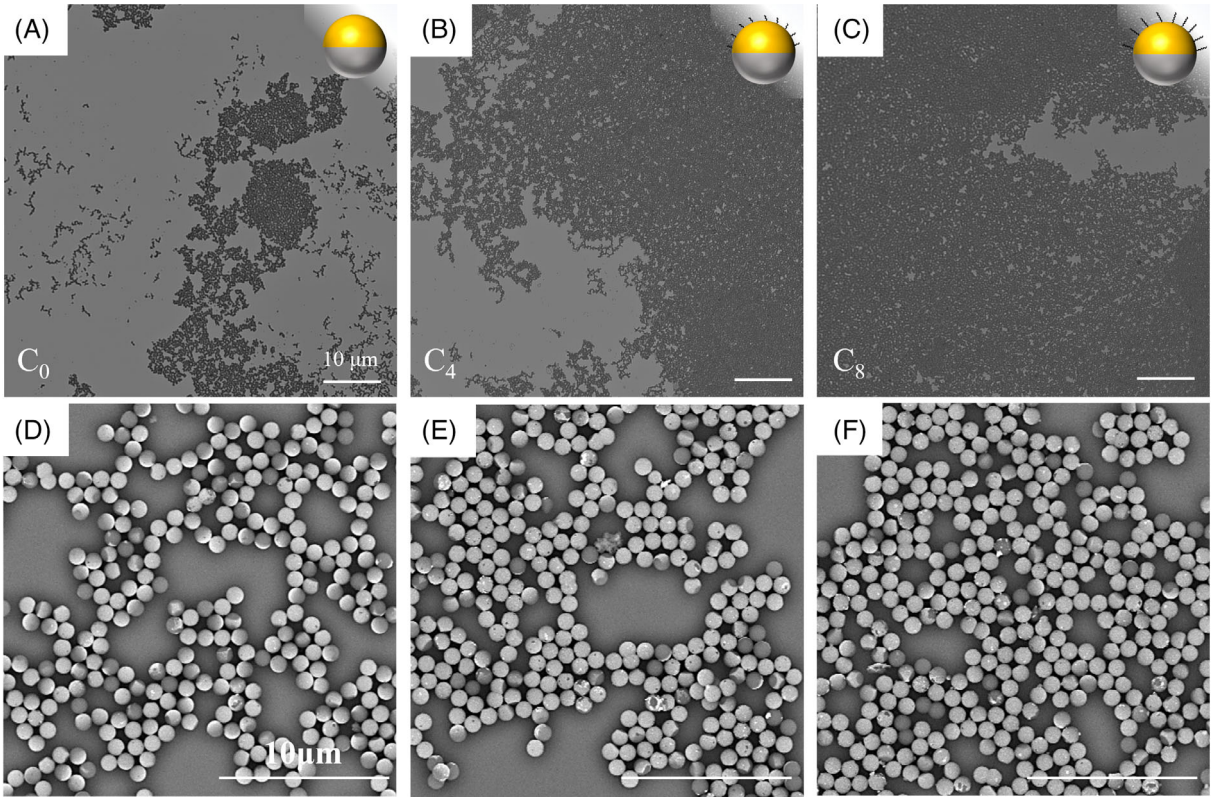

FIGURE 5 Representative optical micrographs of interfacial monolayers formed by (A) C_0, (B) C_4, and (C) C_8 Janus particles of different amphiphilicity. Representative SEM pictures of the clusters formed by the Janus particles of different amphiphilicity (D) C_0, (E) C_4, (F) C_8. Images belong to monolayers at 5 mN/m. Scale bar is 10 μm.

amphiphilicity when compared at similar surface pressures. Furthermore, Figure S6 shows a comparison between the obtained microstructures across different surface pressures and at a similar surface coverage; while the structure formed by C_0 particles exhibit more openings within the clusters, the C_8 monolayer depicts a network that is packed more uniformly. The different degree of amphiphilicity present in the particles could impact their orientation at the interface, as further analyzed in the next section, which, in turn, alters the sign and magnitude of the resulting interparticle interactions that govern the assembly of the interfacial network yielding the captured microstructures.

The SEM images of the monolayers are used to further investigate the role of particle amphiphilicity on the orientation distribution of particles and its connection to the microstructure formation at the interface (Figure 5D–F). The monolayers were deposited onto the silicon wafers at a surface pressure of 5 mN/m. The SEM pictures were used since the gold caps, which appear brighter, can be distinguished from the silica cores. From these images, we observe that not all particles are oriented with their caps pointing upwards, toward the air phase, which is predicted to be the preferred orientation for a single Janus particle residing an interface when the rotational freedom of the particle is not cosidered.[10] It is possible to observe that there is a difference in the number of particles residing at various orientations depending on the degree of amphiphilicity. It is important to note that the process of drying could induce capillary interactions and disturb particle orientations. However, as previously reported, Janus particle clusters tend to maintain their orientation upon drying.[79]

The particle orientation distribution for the three systems was quantified and the results are shown in Figure 6. The percentage of cap up-particles with increasing the JP amphiphilicity improved from 66 ± 2% for C_0 samples to 80 ± 2% for C_8, whereas the number of tilted particles reduced in half. These findings are in agreement with previous results reported elsewhere,[79] where highly amphiphilic particles presented a higher orientational order when compared to homogeneous particles.[65,79,93] In addition, the 2D alignment factor, calculated for the different amphiphilicities, illustrated that the presence of more tilted particles was associated with a less ordered monolayer as there is a direct correlation between S and $\Delta\theta$ (see Table 2). Since the particle orientation distribution is governed by the surface energies between the particle surfaces and the two phases present, the calculations of surface energies were carried out as a function of JP amphiphilicity, and its orientation at the interface, as discussed in the next section.

3.5 | Desorption energy calculations for individual particles at different tilt angles

The role of amphiphilicity in the particle orientation can be assessed by applying the thermodynamics derivation of desorption energy

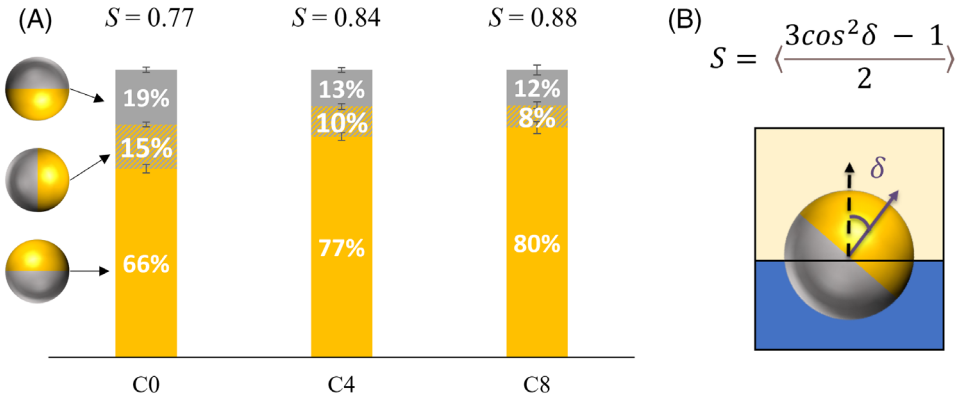

FIGURE 6 (A) Particles orientation distribution for different amphiphilicities. Gold color represents particles residing with their Janus cap aligned with the interface and pointing up toward the air phase, gray pertains to particles sitting with their Janus cap aligned with the interface and pointing down toward the water phase, and the diagonal stripes of gold and gray belong to the particle population with a tilted Janus cap. (B) Schematic showing the orientation angle (δ) and the 2D alignment factor (S).

TABLE 2 The 2D alignment factor (S), the normalized stored energy per particle ($\frac{\Delta U_{cap}}{\pi\sigma_{12}H^2}$), and the corresponding energy in k_bT for monolayers obtained with each particle system.

Particle	S	$\frac{\Delta U_{cap}}{\pi\sigma_{12}H^2}$	$\Delta U_{cap} \times 10^4$ (k_bT)
C_0	0.77	−0.62	−3.5
C_4	0.84	−0.81	−4.6
C_8	0.88	−0.89	−5.1

(Equation 2) to particles at different tilt angles and amphiphilicity. One can calculate the desorption energy assuming that the fluid interface remains flat irrespective of JP tilt angle at the interface (Figure 7A, full lines). However, because of the anisotropy in chemistry present on the surface of Janus particles, one needs to account for the induced deformations of the air–water interface generated by JPs entrapment in a tilted orientation, which affects the resulting wetted areas on each face of the particle. Deformation of fluid interface ensued from JP tilt angle at the interface can be investigated using the Surface Evolver software. Figure 7B illustrates the deformation of the air–water interface in response to a Janus particle trapped at the interface with various tilt angles (δ) for a C_8 particle with $\theta_a = 30^\circ$ and $\theta_p = 100^\circ$. The orientation angle varied from the cap-up orientation (i.e., Janus boundary aligned with the plane of the interface, $\delta = 0^\circ$) to sideways orientation ($\delta = 90^\circ$). These calculations were carried out for all three JPs trapped at different tilt angles at the interface. The change in the desorption energy of the JP, considering the interfacial deformation, is plotted in Figure 7A as a function of JP tilt angle at the interface.

When comparing the calculated desorption energies for particles bound to a flat fluid surface to the scenario where the surface deforms in response to the particle tilt, it should be noted that the deformations of the interface are more thermodynamically favorable since they are associated with more negative desorption energies. Furthermore, for each JP amphiphilicity, the desorption energy becomes less negative as we move from a vertically aligned particle ($\delta = 0^\circ$) to a tilted particle ($\delta = 90^\circ$) indicating that the tilted state is less favorable. Finally, a higher degree of amphiphilicity yields a higher desorption energy for any tilting angle, as expected.

By analyzing the results obtained from the Surface Evolver (Figure 7A, discrete points), it can be noted that the desorption energy is nearly constant for all particles as we move from $\delta = 0^\circ$ up to a critical angle (δ_c) shown by the arrows. C_0 exhibits a higher δ_c, followed by C_4 and C_8, which indicates that C_0 is more likely to assume higher tilt angle at the interface compared to the higher amphiphilicity particles. Moreover, the difference between the desorption energy associated with a particle residing at the interface with a cap-up orientation compared to sideways configuration, with a 90° tilt angle, is directly proportional to the particles amphiphilicity. This attribute can be the driving force for the observed particle orientation distributions (i.e., Figure 6) and how they change with JP amphiphilicity. Under these conditions, we can expect a higher population of particles straddling the interface with their caps oriented upwards for the more amphiphilic system (C_8), as observed from the SEM pictures of Figure 5D–F. Nonetheless, the high count of cap-down particles cannot be explained from thermodynamics point of view, as this configuration is the most energetically unfavorable orientation. We offer two possible explanations for this observation. The first is based on the nonideal fabrication process, where the presence of multilayers in some locations on the substrate could block the particles residing on the lower planes from getting exposed to the metal coating and therefore leave those particles unmodified. The second possibility is that even though these particles are Janus, they might get trapped in a metastable orientation, due to the energetic Marangoni flows associated with their deposition, at the air–water surface. We believe that both possibilities could be taking place in our system.

3.6 | Pairwise capillary interactions

In addition to the impact of amphiphilicity on assumed tilted orientations at the interface, which could result in the deformation of the

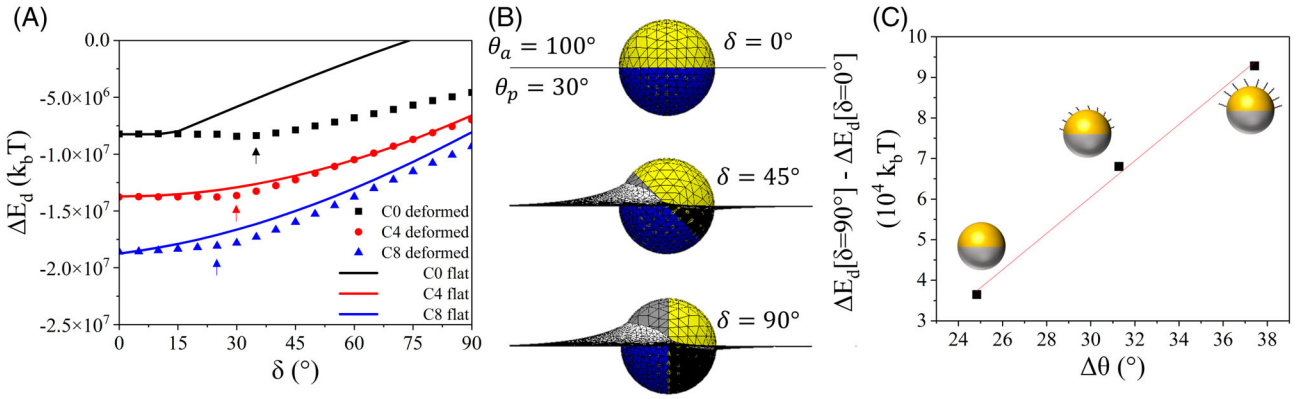

FIGURE 7 (A) Desorption energy (ΔE_d) of an interfacially bound particle calculated for different tilt angles (δ). Full lines represent cases where the surface remains flat regardless of the JP orientation. Discrete points represent results where the deformation of the interface was considered in the calculation of the desorption energy. Results for C_0, C_4, and C_8 particles are shown in black squares, red circles, and blue triangles, respectively. Arrows indicate δ_c for each system. (B) Surface Evolver snapshots and the resulting interfacial deformation induced by the JP tilt angle at the interface displaying a particle with surface characteristics of a C_8 JP on the polar and apolar faces. (C) The difference in the energy required to desorb a tilted JP ΔE_d [$\delta = 90°$] and a cap-up oriented JP ΔE_d [$\delta = 0°$], from the interface, as a function of the degree of amphiphilicity ($\Delta\theta$) of the JPs.

interface, one must also consider the role of particle roughness on interfacial deformation. Since the Janus fabrication method is not seamless (i.e., the Janus boundary introduces surface roughness around the particle), vertically aligned particles (cap up or down) will introduce a contact line deformation that is likely correspondent to the shape of the Janus boundary.[94] These deformations yield capillary interactions between the interfacially bound particles. Previous studies have associated the interactions between these particles to be quadrupolar ($U \propto r^{-4}$) and/or hexapolar ($U \propto r^{-6}$).[65,80] While those higher-order capillary interactions are associated with vertically aligned particles, tilted JPs can also be present on the monolayer (see Figure 5D–F), which adds the dipolar mode of interaction ($U \propto r^{-2}$) to the system. In addition, defects on the Janus boundary may also induce complexity on the pinning of the contact line around the particle surface. All of the beforementioned factors contribute to a unique and complex monolayer at the interface and need to be taken into consideration.

As mentioned earlier, interactions between nontilted JPs can be estimated with quadrupolar and hexapolar interaction modes. These interactions result in different packing arrangements; where quadrupolar dominated systems will form square ordered clusters, hexapolar dominated monolayers will assemble in a hexagonal arrangement.[60,80] For our system, we observe amorphous clusters, with occurrences of both arrangements locally (see Figure S3a). The presence of tilted particles also impacts the overall packing, which makes it nontrivial to determine a dominant mode of capillary interaction. One way of approaching this problem is to analyze the bond angles between neighboring particles to investigate whether either squared or hexagonal arrangements are more frequent.[95] From the analysis carried out in Figure S3c, it can be seen that for all the systems under study in this work, there is a higher tendency of finding pairs with bond angles of 60° and 120°, which originate from a hexagonal arrangement even though the microstructure is overall amorphous, as seen in Figure 5D–F. Therefore, for the sake of simplicity, further analysis of these JP systems was carried out with the assumption that the vertically aligned particles ($\delta = 0°$) deform the contact line predominantly by a hexapolar mode. It should be noted that quadrupoles are likely to be present in the monolayers as well.

As shown in Equation (3), capillary interactions depend on the approach angle between the particles. When looking into a pair of similarly oriented particles, we can estimate the pair-interaction potential dependence on the azimuthal angle (or approach angle, $\Delta\varphi$). For a pair of particles deforming the interface in a hexapolar fashion, the radial interaction map calculated using Equation (3) for different center to center distances (r) and approach angles ($\Delta\varphi$), is shown in Figure 8A. The values shown in the figure represent the total interaction energy (ΔU_{cap}) normalized by the surface tension (σ) and the squared deformation amplitude (H^2) assuming $\sigma_{12} = 72.8$ mN/m and $H = 32$ nm. For our system, H was estimated based on the roughness of the core particle and the roughness introduced by the metal deposition, following the work of Qiao et al.[78] It is possible to notice that there are three attractive and three repulsive domains, as expected. Therefore, in a dilute regime (i.e., low particle surface coverage), when two particles approach each other in a favorable configuration (i.e., deformation modes are matching), attraction will be ensued. If the particles approach each other in a unfavorable configuration, assuming they are free to rotate in plane (radial movement on the graph), they can align their deformations and switch to the attraction region of the capillary interaction map.[43,96] For instance, in a system composed of two particles interacting via hexapolar capillary interactions, the maximum in-plane rotation needed for a single particle to switch the interaction potential sign, and move from maximum repulsion to maximum attraction, is 60°. Figure 8B shows a similar scenario for two tilted particles deforming the interface in a dipolar fashion. In comparison to the previous case, two tilted particles approaching each

other in the most unfavorable orientation may need to rotate up to (180°) to move from a repulsive domain toward an attractive range. For a dilute system (i.e., low particle surface coverage) this is not an issue. However, when considering populated surfaces, a complicated network of interactions arises from the many-body interactions, which could constrain the in-plane rotations.

From Figure 8, we can determine two possible scenarios for each particle pair: the most attractive and the most repulsive paths, which depend on the alignment of the surface deformations that are caused by these particles. These scenarios are illustrated in Figure 9A,B for particles interacting solely via hexapolar or dipolar modes, respectively. For cap up particles interacting via hexapolar mode (Figure 9A),

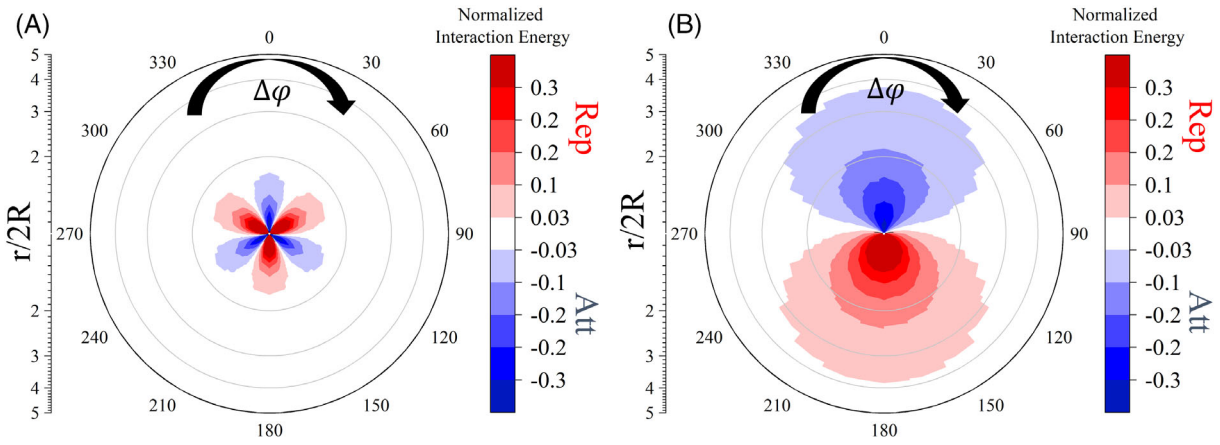

FIGURE 8 Radial map of normalized pairwise capillary interaction for two particles as a function of center-to-center separation distance (r) normalized by particle diameter ($2R$) distances and their in-plane approach angle ($\Delta\varphi$). (A) Two particles interacting through (A) hexapolar and (B) dipolar capillary interactions. Regions shown in red (blue) represent repulsive (attractive) capillary interactions.

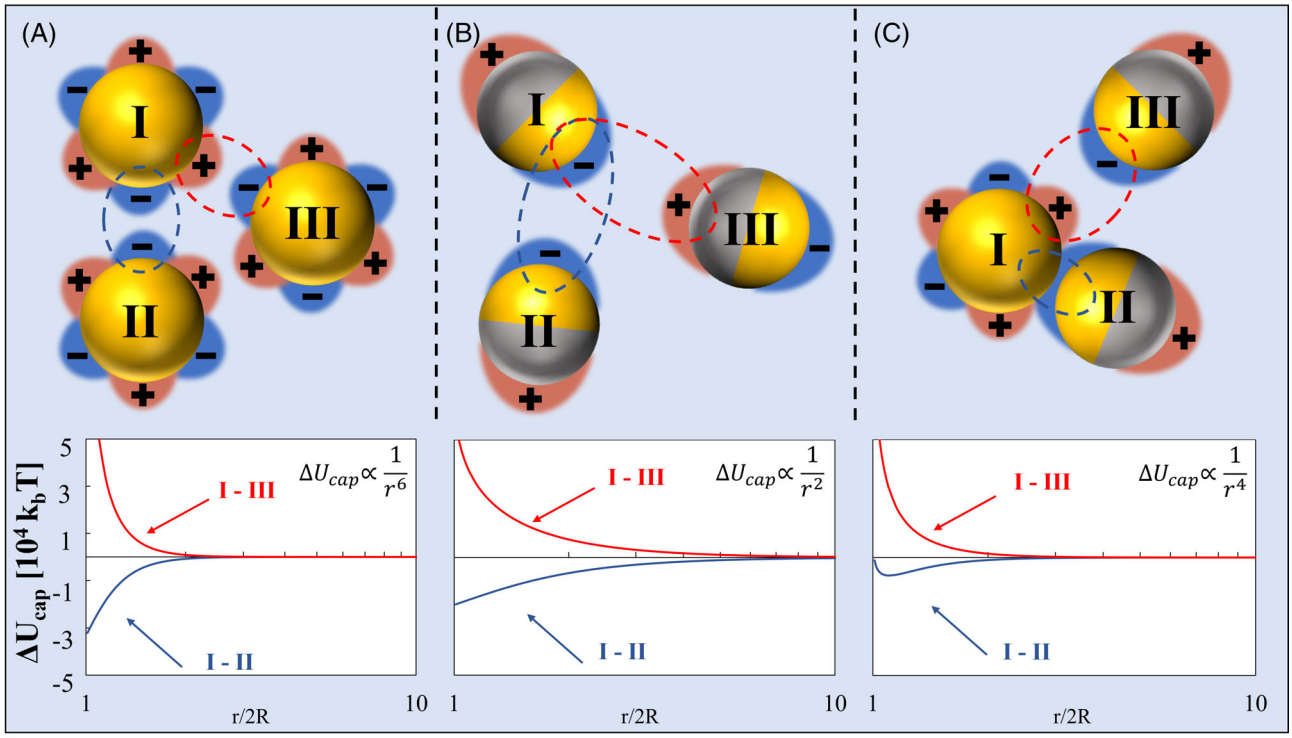

FIGURE 9 Cartoons showing the top-view of three particles trapped at the air–water interface, where upward (downward) surface deformations are represented as a plus (minus) sign and in red (blue) color. Capillary interactions resulting between two pairs are provided in the bottom panel for particles interacting either attractively (particles I and II) or repulsively (particles I and III) and are as follows: (A) hexapolar–hexapolar, (B) dipolar–dipolar, and (C) hexapolar–dipolar. Scaling of capillary interactions with separation distance for each scenario is provided on the plots. Interaction curves were calculated based on the numerical solution provided by Kralchesvky et al. for multipolar capillary interactions.[60]

they may experience an attraction (particles IA–IIA) or a repulsion (particles IA–IIIA) depending on how they approach each other. For tilted particles interacting via dipolar mode (Figure 9B), we have a similar scenario where matching deformations are attractive (particles IB–IIB) and opposing deformations are repulsive (particles IB–IIIB). It is also possible to observe that at smaller separation distances, vertically aligned particles interact strongly, while the capillary interaction between tilted particles is longer ranged.

The interaction potential between a vertically-aligned particle and a tilted particle is not trivial, even under the simplifying assumption that upright particles do not deform the interface (i.e., smooth Janus boundary), as shown previously by Rezvantalab et al.[43] When considering that vertically-aligned particles deform the surface in a hexapolar fashion, we arrive at a scenario with interaction profile depicted in Figure 9C. For the attractive pair (IC–IIC), at large distances, the particles are attracted to each other, however their interaction energy reaches a minimum before reaching close contact. Upon further reduction in separation distance, particles start repelling each other. This can be explained by acknowledging that when moving a hexapolar particle closer to a dipolar particle, there is a distance at which opposing deformations will overlap because the dipolar deformations are wider than the hexapolar ones. This is exemplified by the pair IC–IIC in Figure 9C, where the downwards interfacial deformation around the dipolar particle matches the downwards deformation on the hexapolar particle. Nevertheless, if the particles keep approaching each other, the downwards deformation of the dipolar particle will overlap with the upwards deformations on the hexapolar particle, which is not an energetically favorable state, as it increases the interfacial contact area between the two fluids.

We have further analyzed the SEM pictures to examine pairwise interactions present in monolayers formed by each particle amphiphilicity and for the different particle orientations. This can be conducted by setting a threshold distance that characterizes the first shell of neighbors (analysis can be found in Figure S4), followed by counting each detected pair and comparing their assigned orientations to get the number of interactions between each case (up–up, up–tilted, etc.). As shown in Figure 10, majority of interactions are between particles possessing cap up configuration, as expected. When considering C_0 JPs, ~21.0% of the interparticle interactions are between the cap-up and tilted particles, in contrast to only ~12.5% for C_8 JPs. This indicates that within C_0 monolayer, there is a higher recurrence rate of the complex scenario shown in Figure 9C. This is indeed expected as the higher number of tilted particles are present in the interfacial network formed by C_0 particles, as displayed in Figure 6A, which in turn results in a higher chance of interactions involving them.

Once the interacting pairs are identified, the pairwise interaction experienced by each particle can be calculated in order to determine the network of interactions present in each system. An assumption that was made in these calculations was that the amplitude of deformation is constant regardless of the particle orientation within the monolayer. Since upwards and downwards surface deformations around vertically aligned particles cannot be distinguished from an SEM image, we also assume that these particles are always in the most attractive configuration with respect to their pairs. Therefore, pairs containing at least one vertical particle will follow the attractive capillary interaction scenarios (blue curves) shown in Figure 9A,B. For a pair of tilted particles, the sign of interfacial deformation can be determined based on the cap direction and used in calculating the magnitude and sign of the pairwise capillary interaction.

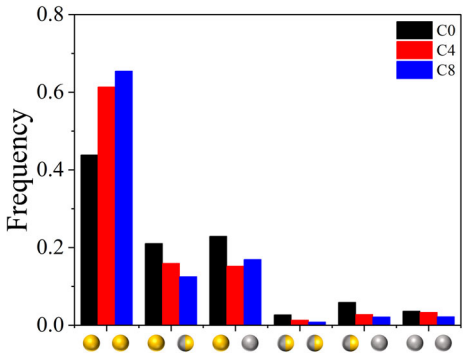

FIGURE 10 Frequency of pairwise interactions for pairs of different orientations as a function of JP amphiphilicity. From left to right, up–up, up–tilted, up–down, tilted–tilted, tilted–down, down–down. Data belonging to C_0, C_4, and C_8 particles are shown in black, red, and blue color, respectively. The data was obtained from SEM images of monolayers deposited at 5 mN/m.

Figure 11 shows the normalized particle interaction energy as a Voronoi diagram, where area surrounding each particle is colored with respect to the amount of capillary interaction energy corresponding to that particle resulting from its neighbors. The corresponding SEM images used in the analysis of Figure 11 can be found in Figure S5. It is worth noting that the cluster formed by C_0 particles depicts a higher occurrence of repulsive interactions (colored in red) when compared to the C_8 cluster, which is dominated by attractive interactions (blue).

From the capillary interaction energy values calculated for each particle within the cluster, we can estimate an average energy stored per particle (ΔU_{cap}), results of which are provided in Table 2. There is a direct correlation between the interaction energy (ΔU_{cap}) and the JP amphiphilicity ($\Delta\theta$). All amphiphilicities yielded attractive interaction energies, which is expected for a cluster that was self-assembled at the air–water interface. These results are in agreement with the physics obtained from the fitting of the isotherms, where C_8 particles were found to exhibit stronger attractive interactions ($a = 1.09$) compared to the other two amphiphilicities.

It should be noted that a number of assumptions were made in the beforementioned calculations, as follows: (1) cap-down particles are equivalent to cap-up particles in the calculation of pairwise interaction, which might not be true if those particles are indeed homogeneous untreated particles and not cap-down Janus particles; (2) all amphiphilicities considered in this study will result in the deformation of the surface with the same amplitude, whereas the deformation should be dependent on the degree of amphiphilicity;[43] (3) tilted particles are deforming the surface with the same amplitude as the vertical ones; (4) the depression and rise of the fluid interface, resulting from tilted particles at the interface, are of the same

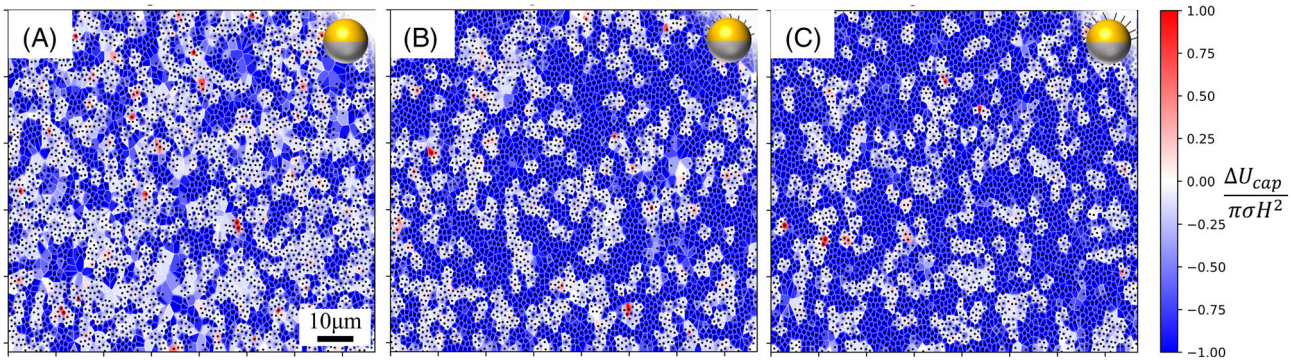

FIGURE 11 Voronoi diagram for particle clusters within (A) C_0, (B) C_4, (C) C_8 monolayers. The particles centers a shown using black dots, and the area surrounding each particle is colored with respect to the energy resulting from the summation of interactions with its neighbors. The monolayers were deposited at 5 mN/m.

magnitude; and (5) defects from the particle fabrication may introduce various modes of capillary deformations (e.g., quadrupolar) that are not considered in the calculations presented in this study. We are currently investigating the impact of these factors on the resulting capillary interactions, which will be the subject of a forthcoming publication.

4 | CONCLUSIONS

To shed light on the role JP amphiphilicity plays in the formation of an interfacial microstructure and its mechanical properties, in this work, we examined JP monolayers of different amphiphilicity subjected to compression and expansion stresses. The analysis was carried out via the measurement of surface pressure isotherms followed by their characterization with an equation of state to highlight the impact of JP amphiphilicity on the resulting interparticle interactions. We further analyzed the role of JP amphiphilicity on the microstructure formation by determining the orientation distribution of JPs at the interface from the images of the particle networks at the air–water interface. We employed Surface Evolver software to estimate the desorption energy associated with such interfacially bound JPs, trapped at different orientation angles with regards to the interface, to underscore the importance of particle amphiphilicity. We found that for higher amphiphilicity JPs, there is a larger energy penalty for particles to assume a tilted orientation at the interface in comparison to those vertically aligned. We postulated that the different orientation distribution captured for various degrees of JP amphiphilicity, dictates the modes of capillary interactions that are present within the monolayer. When comparing JPs of different amphiphilicities, we conclude that the capillary interactions induced by the tilted JPs at the interface and the resulting interfacial deformations are the main contributing factor to such different self-assembly behavior at the air–water surface and the accompanying response to the applied compression, which is of significance for designing interfacial systems for industrial applications.

Tuning the rheological properties of interfacial networks by engineering the particle attributes that form the monolayer has been envisioned in the field. For example, the rheological properties of interfacial monolayers formed by ellipsoidal particles, such as their yield point, was reported to be higher at similar surface coverages when compared to spherical particles, which in turn has been shown to arrest bubble dissolution, a useful attribute in designing stable Pickering foams.[97] Moreover, the surface pressure of JPs monolayers have also been shown to impact their resulting interfacial rheology.[98] Consequentially, this illustrates the opportunity to use the capillary interactions as a tool to tune the properties of interfacial systems.[99,100] Understanding these concepts is key in designing interfacial systems, by engineering the surface attributes of particles, and is essential for numerous applications of soft-matter, as listed in the New Directions for Chemical Engineering.[101]

AUTHOR CONTRIBUTIONS

Elton Correia: Data curation (lead); formal analysis (lead); investigation (equal); methodology (equal); visualization (lead); writing – original draft (lead). **Sepideh Razavi:** Conceptualization (lead); funding acquisition (lead); investigation (lead); methodology (equal); project administration (lead); resources (lead); supervision (lead); writing – review and editing (lead).

ACKNOWLEDGMENTS

SR and EC would like to thank Prof. James Gilchrist from Lehigh University for providing the PVC sheets coated with the silica particles, which were then used in the fabrication of Janus particles in our lab. SR and EC would like to thank Prof. Ken Brakke for the assistance with the Surface Evolver simulations. EC acknowledges the support of the National Association for Surface Finishing (NASF) for the graduate scholarship and the Gallogly College of Engineering Dissertation Excellence Award. SR and EC acknowledge the support from the National Science Foundation through the award CBET-1934513 and the NSF-CAREER award CBET-2144020.

CONFLICT OF INTEREST STATEMENT

The authors declare no competing financial interest.

DATA AVAILABILITY STATEMENT

The numerical data from Figures 2–4, 7–10, S1, S3, and S4 are tabulated in Supporting Information as spreadsheets. Error bars shown on contact angle measurements are from the standard deviation of at least 20 droplets measured independently. The Langmuir trough measurements were performed at least 3-times and their derivative was used to calculate the spread associated with the surface compressibility factor shown in Table 1. Image analysis was performed on at least 20 images taken at different positions for each amphiphilicity, where roughly 50,000 particles were characterized and used to calculate the orientation distribution shown in Figure 6.

ORCID

Sepideh Razavi https://orcid.org/0000-0003-1225-6081

REFERENCES

1. Ramsden W. Separation of solids in the surface-layers of solutions and 'suspensions' (observations on surface-membranes, bubbles, emulsions, and mechanical coagulation)—preliminary account. *Proc R Soc Lond*. 1904;72(477–486):156-164.
2. Pickering SU. CXCVI—emulsions. *J Chem Soc Trans*. 1907;91:2001-2021.
3. Mendoza AJ, Guzmán E, Martínez-Pedrero F, et al. Particle laden fluid interfaces: dynamics and interfacial rheology. *Adv Colloid Interface Sci*. 2014;206:303-319.
4. Binks BP, Horozov TS. *Colloidal Particles at Liquid Interfaces*. Cambridge University Press; 2006.
5. Aveyard R, Binks BP, Clint JH. Emulsions stabilised solely by colloidal particles. *Adv Colloid Interface Sci*. 2003;100–102:503-546.
6. Chen CL, Wang SS, Kadhum MJ, Harwell JH, Shiau BJ. Using carbonaceous nanoparticles as surfactant carrier in enhanced oil recovery: a laboratory study. *Fuel*. 2018;222:561-568.
7. Liu RC, Raman AKY, Shaik I, Aichele C, Kim SJ. Inorganic microfiltration membranes incorporated with hydrophilic silica nanoparticles for oil-in-water emulsion separation. *J Water Process Eng*. 2018;26:124-130.
8. Ballard N, Law AD, Bon SAF. Colloidal particles at fluid interfaces: behaviour of isolated particles. *Soft Matter*. 2019;15(6):1186-1199.
9. Razavi S, Lin B, Lee KYC, Tu RS, Kretzschmar I. Impact of surface amphiphilicity on the interfacial behavior of Janus particle layers under compression. *Langmuir*. 2019;35:15813-15824.
10. Binks BP, Fletcher PDI. Particles adsorbed at the oil−water Interface: a theoretical comparison between spheres of uniform wettability and "Janus" particles. *Langmuir*. 2001;17(16):4708-4710.
11. Pieranski P. Two-dimensional interfacial colloidal crystals. *Phys Rev Lett*. 1980;45(7):569-572.
12. Park BJ, Lee D. Particles at fluid–fluid interfaces: from single-particle behavior to hierarchical assembly of materials. *MRS Bull*. 2014;39(12):1089-1098.
13. Kaz DM. *Colloidal Particles and Liquid Interfaces: A Spectrum of Interactions*. PhD thesis. Harvard University; 2011.
14. Zang DY, Rio E, Langevin D, Wei B, Binks BP. Viscoelastic properties of silica nanoparticle monolayers at the air–water interface. *Eur Phys J E*. 2010;31(2):125-134.
15. Komura S, Hirose Y, Nonomura Y. Adsorption of colloidal particles to curved interfaces. *J Chem Phys*. 2006;124(24):241104.
16. Bresme F, Oettel M. Nanoparticles at fluid interfaces. *J Phys Condens Matter*. 2007;19(41):413101.
17. Vishal B, Ghosh P. The effect of silica nanoparticles on the stability of aqueous foams. *J Dispers Sci Technol*. 2019;40(2):206-218.
18. Hu N, Li Y, Wu Z, Lu K, Huang D, Liu W. Foams stabilization by silica nanoparticle with cationic and anionic surfactants in column flotation: effects of particle size. *J Taiwan Inst Chem Eng*. 2018;88:62-69.
19. Weston JS, Jentoft RE, Grady BP, Resasco DE, Harwell JH. Silica nanoparticle wettability: characterization and effects on the emulsion properties. *Ind Eng Chem Res*. 2015;54(16):4274-4284.
20. Zhou J, Qiao X, Binks BP, et al. Magnetic pickering emulsions stabilized by Fe_3O_4 nanoparticles. *Langmuir*. 2011;27(7):3308-3316.
21. Owoseni O, Nyankson E, Zhang Y, et al. Interfacial adsorption and surfactant release characteristics of magnetically functionalized halloysite nanotubes for responsive emulsions. *J Colloid Interface Sci*. 2016;463:288-298.
22. Xue Z, Worthen A, Qajar A, et al. Viscosity and stability of ultra-high internal phase CO_2-in-water foams stabilized with surfactants and nanoparticles with or without polyelectrolytes. *J Colloid Interface Sci*. 2016;461:383-395.
23. Arab D, Kantzas A, Bryant SL. Nanoparticle stabilized oil in water emulsions: a critical review. *J Petrol Sci Eng*. 2018;163:217-242.
24. Katepalli H, Bose A. Response of surfactant stabilized oil-in-water emulsions to the addition of particles in an aqueous suspension. *Langmuir*. 2014;30(43):12736-12742.
25. Fan H, Striolo A. Mechanistic study of droplets coalescence in pickering emulsions. *Soft Matter*. 2012;8(37):9533-9538.
26. Hunter T, Pugh R, Franks G, Jameson G. The role of particles in stabilising foams and emulsions. *Adv Colloid Interface Sci*. 2008;137:57-81.
27. Tu F, Lee D. Shape-changing and amphiphilicity-reversing Janus particles with pH-responsive surfactant properties. *J Am Chem Soc*. 2014;136(28):9999-10006.
28. McConnell MD, Kraeutler MJ, Yang S, Composto RJ. Patchy and multiregion janus particles with tunable optical properties. *Nano Lett*. 2010;10(2):603-609.
29. Agrawal G, Agrawal R. Janus nanoparticles: recent advances in their interfacial and biomedical applications. *ACS Appl Nano Mater*. 2019;2(4):1738-1757.
30. Van Hooghten R, Imperiali L, Boeckx V, Sharma R, Vermant J. Rough nanoparticles at the oil–water interfaces: their structure, rheology and applications. *Soft Matter*. 2013;9(45):10791-10798.
31. Liu J, Li X, Jia W, Li Z, Zhao Y, Ren S. Demulsification of crude oil-in-water emulsions driven by graphene oxide nanosheets. *Energy Fuel*. 2015;29(7):4644-4653.
32. Pawar AB, Caggioni M, Hartel RW, Spicer PT. Arrested coalescence of viscoelastic droplets with internal microstructure. *Faraday Discuss*. 2012;158:341-350.
33. Sacanna S, Korpics M, Rodriguez K, et al. Shaping colloids for self-assembly. *Nat Commun*. 2013;4(1):1688.
34. Vu TV, Papavassiliou DV. Modification of oil–water interfaces by surfactant-stabilized carbon nanotubes. *J Phys Chem C*. 2018;122(48):27734-27744.
35. Raphaël E, Di Meglio J-M, Berger M, Calabi E. Convex particles at interfaces. *J Phys I*. 1992;2(5):571-579.
36. Ondarçuhu T, Fabre P, Raphaël E, Veyssié M. Specific properties of amphiphilic particles at fluid interfaces. *J Phys France*. 1990;51(14):1527-1536.
37. di Meglio J, Raphael E. Equilibrium of a spherical particle at a curved liquid/liquid interface. *J Colloid Interface Sci*. 1990;136(2):581-583.
38. Jiang S, Granick S. Janus balance of amphiphilic colloidal particles. *J Chem Phys*. 2007;127(16):161102.
39. Gao Y, Yu Y. Macrophage uptake of Janus particles depends upon Janus balance. *Langmuir*. 2015;31(9):2833-2838.
40. Correia EL, Brown N, Razavi S. Janus particles at fluid interfaces: stability and interfacial rheology. *Nanomaterials*. 2021;11(2):374.
41. Cheung DL, Bon SA. Stability of Janus nanoparticles at fluid interfaces. *Soft Matter*. 2009;5(20):3969-3976.

42. Park BJ, Lee D. Equilibrium orientation of nonspherical Janus particles at fluid–fluid interfaces. *ACS Nano*. 2012;6(1):782-790.
43. Rezvantalab H, Shojaei-Zadeh S. Role of geometry and amphiphilicity on capillary-induced interactions between anisotropic Janus particles. *Langmuir*. 2013;29(48):14962-14970.
44. Bleibel J, Domínguez A, Oettel M. Colloidal particles at fluid interfaces: effective interactions, dynamics and a gravitation–like instability. *Eur Phys J Special Top*. 2013;222(11):3071-3087.
45. Correia EL, Thakur S, Ervin A, Shields E, Razavi S. Adsorption of surfactant molecules onto the surface of colloidal particles: case of like-charged species. *Colloids Surf A Physicochem Eng Asp*. 2023;676:132142.
46. Hurd AJ. The electrostatic interaction between interfacial colloidal particles. *J Phys A Math Gen*. 1985;18(16):L1055-L1060.
47. Girotto M, dos Santos AP, Levin Y. Interaction of charged colloidal particles at the air–water Interface. *J Phys Chem B*. 2016;120(26):5817-5822.
48. Park BJ, Vermant J, Furst EM. Heterogeneity of the electrostatic repulsion between colloids at the oil–water interface. *Soft Matter*. 2010;6(21):5327-5333.
49. Aveyard R, Binks BP, Clint JH, et al. Measurement of long-range repulsive forces between charged particles at an oil-water Interface. *Phys Rev Lett*. 2002;88(24):246102.
50. Park BJ, Pantina JP, Furst EM, Oettel M, Reynaert S, Vermant J. Direct measurements of the effects of salt and surfactant on interaction forces between colloidal particles at water—oil interfaces. *Langmuir*. 2008;24(5):1686-1694.
51. Oettel M, Dietrich S. Colloidal interactions at fluid interfaces. *Langmuir*. 2008;24(4):1425-1441.
52. Park BJ, Furst EM. Attractive interactions between colloids at the oil–water interface. *Soft Matter*. 2011;7(17):7676-7682.
53. Hurd A. The electrostatic interaction between interfacial colloidal particles. *J Phys A Math Gen*. 1999;18:L1055-L1060.
54. Wirth CL, Furst EM, Vermant J. Weak electrolyte dependence in the repulsion of colloids at an oil–water interface. *Langmuir*. 2014;30(10):2670-2675.
55. Israelachvili JN. 6 – Van der Waals forces. In: Israelachvili JN, ed. *Intermolecular and Surface Forces (Third Edition)*. Academic Press; 2011:107-132.
56. Shemi O, Solomon MJ. Effect of surface chemistry and metallic layer thickness on the clustering of metallodielectric Janus spheres. *Langmuir*. 2014;30(51):15408-15415.
57. Tsyrenova A, Miller K, Yan J, Olson E, Anthony SM, Jiang S. Surfactant-mediated assembly of amphiphilic Janus spheres. *Langmuir*. 2019;35(18):6106-6111.
58. Kralchevsky PA, Paunov VN, Ivanov IB, Nagayama K. Capillary meniscus interaction between colloidal particles attached to a liquid—fluid interface. *J Colloid Interface Sci*. 1992;151(1):79-94.
59. Paunov VN, Kralchevsky PA, Denkov ND, Nagayama K. Lateral capillary forces between floating submillimeter particles. *J Colloid Interface Sci*. 1993;157(1):100-112.
60. Danov KD, Kralchevsky PA, Naydenov BN, Brenn G. Interactions between particles with an undulated contact line at a fluid interface: capillary multipoles of arbitrary order. *J Colloid Interface Sci*. 2005;287(1):121-134.
61. Kralchevsky PA, Nagayama K. Capillary interactions between particles bound to interfaces, liquid films and biomembranes. *Adv Colloid Interface Sci*. 2000;85(2):145-192.
62. Stamou D, Duschl C, Johannsmann D. Long-range attraction between colloidal spheres at the air–water interface: the consequence of an irregular meniscus. *Phys Rev E*. 2000;62(4):5263-5272.
63. Goggin DM, Samaniuk JR. Dynamics of pristine graphite and graphene at an air–water interface. *AIChE J*. 2018;64(8):3177-3187.
64. Vella D, Mahadevan L. The "cheerios effect". *Am J Phys*. 2005;73(9):817-825.
65. Park B, Brugarolas T, Lee D. Janus particles at an oil–water interface. *Soft Matter*. 2011;7:6413-6417.
66. Hashmi S, Wickman H, Weitz D. Tetrahedral calcite crystals facilitate self-assembly at the air–water interface. *Phys Rev E*. 2005;72(4):041605.
67. Kralchevsky PA, Nagayama K. Capillary forces between colloidal particles. *Langmuir*. 1994;10(1):23-36.
68. Danov KD, Kralchevsky PA, Boneva MP. Electrodipping force acting on solid particles at a fluid interface. *Langmuir*. 2004;20(15):6139-6151.
69. Nikolaides MG, Bausch AR, Hsu MF, et al. Electric-field-induced capillary attraction between like-charged particles at liquid interfaces. *Nature*. 2002;420(6913):299-301.
70. Lewandowski EP, Cavallaro M, Botto L, Bernate JC, Garbin V, Stebe KJ. Orientation and self-assembly of cylindrical particles by anisotropic capillary interactions. *Langmuir*. 2010;26(19):15142-15154.
71. Kang DW, Choi KH, Lee SJ, Park BJ. Mapping anisotropic and heterogeneous colloidal interactions via optical laser tweezers. *J Phys Chem Lett*. 2019;10(8):1691-1697.
72. Liu IB, Sharifi-Mood N, Stebe KJ. Capillary assembly of colloids: interactions on planar and curved interfaces. *Annu Rev Condens Matter Phys*. 2018;9(1):283-305.
73. Thakur S, Razavi S. Particle size and rheology of silica particle networks at the air–water Interface. *Nanomaterials*. 2023;13(14):2114.
74. Botto L, Lewandowski EP, Cavallaro M, Stebe KJ. Capillary interactions between anisotropic particles. *Soft Matter*. 2012;8(39):9957-9971.
75. Trevenen S, Hamilton HS, Ribbe AE, Bradley LC, Beltramo PJ. Nanoscale porosity in microellipsoids cloaks interparticle capillary attraction at fluid interfaces. *ACS Nano*. 2022;17(12):11892-11904.
76. Wang A, Rogers WB, Manoharan VN. Effects of contact-line pinning on the adsorption of nonspherical colloids at liquid interfaces. *Phys Rev Lett*. 2017;119(10):108004.
77. Brugarolas T, Park B, Lee M, Lee D. Generation of amphiphilic Janus bubbles and their behavior at an air–water interface. *Adv Funct Mater*. 2011;21:3924-3931.
78. Qiao Y, Ma X, Liu Z, Manno MA, Keim NC, Cheng X. Tuning the rheology and microstructure of particle-laden fluid interfaces with Janus particles. *J Colloid Interface Sci*. 2022;618:241-247.
79. Miller K, Tsyrenova A, Anthony SM, Qin S, Yong X, Jiang S. Drying mediated orientation and assembly structure of amphiphilic Janus particles. *Soft Matter*. 2018;14(33):6793-6798.
80. Carrasco-Fadanelli V, Castillo R. Measurement of the capillary interaction force between Janus colloidal particles trapped at a flat air/-water interface. *Soft Matter*. 2020;16(25):5910-5914.
81. Adams DJ, Adams S, Melrose J, Weaver AC. Influence of particle surface roughness on the behaviour of Janus particles at interfaces. *Colloids Surf A Physicochem Eng Asp*. 2008;317(1):360-365.
82. Lucassen J. Capillary forces between solid particles in fluid interfaces. *Colloids Surf*. 1992;65(2):131-137.
83. Yao L, Botto L, Cavallaro JM, Bleier BJ, Garbin V, Stebe KJ. Near field capillary repulsion. *Soft Matter*. 2013;9(3):779-786.
84. Li X, Gilchrist JF. Large-area nanoparticle films by continuous automated Langmuir–Blodgett assembly and deposition. *Langmuir*. 2016;32(5):1220-1226.
85. Brown N, de la Pena A, Razavi S. Interfacial rheology insights: particle texture and Pickering foam stability. *J Phys Condens Matter*. 2023;35:384002. doi:10.1088/1361-648X/acde2c
86. Fainerman V, Kovalchuk V, Lucassen-Reynders E, et al. Surface-pressure isotherms of monolayers formed by microsize and nanosize particles. *Langmuir*. 2006;22(4):1701-1705.

87. Domonkos M, Jackivová R, Pathó A. Image analysis algorithm for the verification of hexagonal symmetry in spherical nanostructures. *Microelectron Eng*. 2022;251:111635.
88. Vu TV, Razavi S, Papavassiliou DV. Effect of Janus particles and non-ionic surfactants on the collapse of the oil-water interface under compression. *J Colloid Interface Sci*. 2022;609:158-169.
89. Brakke KA. The Surface Evolver. *Exp Math*. 1992;1(2):141-165.
90. Razavi S, Cao KD, Lin B, Lee KYC, Tu RS, Kretzschmar I. Collapse of particle-laden interfaces under compression: buckling vs particle expulsion. *Langmuir*. 2015;31(28):7764-7775.
91. Bykov A, Noskov B, Loglio G, Lyadinskaya V, Miller R. Dilational surface elasticity of spread monolayers of polystyrene microparticles. *Soft Matter*. 2014;10(34):6499-6505.
92. Da C, Zhang X, Alzobaidi S, Hu D, Wu P, Johnston KP. Tuning surface chemistry and ionic strength to control nanoparticle adsorption and elastic dilational modulus at air–brine interface. *Langmuir*. 2021;37(19):5795-5809.
93. Knapp E. *Janus Particles at the Air–Water Interface: Single Particle Behavior, Particle-Laden Interfaces, and Implications for Self-Assembly*. The City College of New York; 2019.
94. Wang X, In M, Blanc C, Malgaretti P, Nobili M, Stocco A. Wetting and orientation of catalytic Janus colloids at the surface of water. *Faraday Discuss*. 2016;191:305-324.
95. Goggin DM, Samaniuk JR. 2D colloids: size-and shape-controlled 2D materials at fluid–fluid interfaces. *Langmuir*. 2021;37(48):14157-14166.
96. Jeong HW, Park JW, Lee HM, et al. Retardation of capillary force between Janus particles at the oil–water interface. *J Phys Chem Lett*. 2022;13(42):10018-10024.
97. Beltramo PJ, Gupta M, Alicke A, et al. Arresting dissolution by interfacial rheology design. *Proc Natl Acad Sci U S A*. 2017;114(39):10373-10378.
98. Correia EL, Winter HH, Razavi S. Two-dimensional glass transition–like behavior of Janus particle–laden interface. *Rheol Acta*. 2023;62:1-13.
99. Barman S, Christopher GF. Role of capillarity and microstructure on interfacial viscoelasticity of particle laden interfaces. *J Rheol*. 2016;60(1):35-45.
100. Rahman SE, Laal-Dehghani N, Barman S, Christopher GF. Modifying interfacial interparticle forces to alter microstructure and viscoelasticity of densely packed particle laden interfaces. *J Colloid Interface Sci*. 2019;536:30-41.
101. National Academies of Sciences, Engineering, and Medicine. *New Directions for Chemical Engineering*. The National Academies Press; 2022.

SUPPORTING INFORMATION

Additional supporting information can be found online in the Supporting Information section at the end of this article.

How to cite this article: Correia EL, Razavi S. Janus particle amphiphilicity and capillary interactions at a fluid interface. *AIChE J*. 2023;69(12):e18241. doi:10.1002/aic.18241